Quadrupole NMR

Marina Carravetta (marina@soton.ac.uk)

School of Chemistry, University of Southampton

March 24, 2014

Outline

Nuclear spin and periodic table (1)

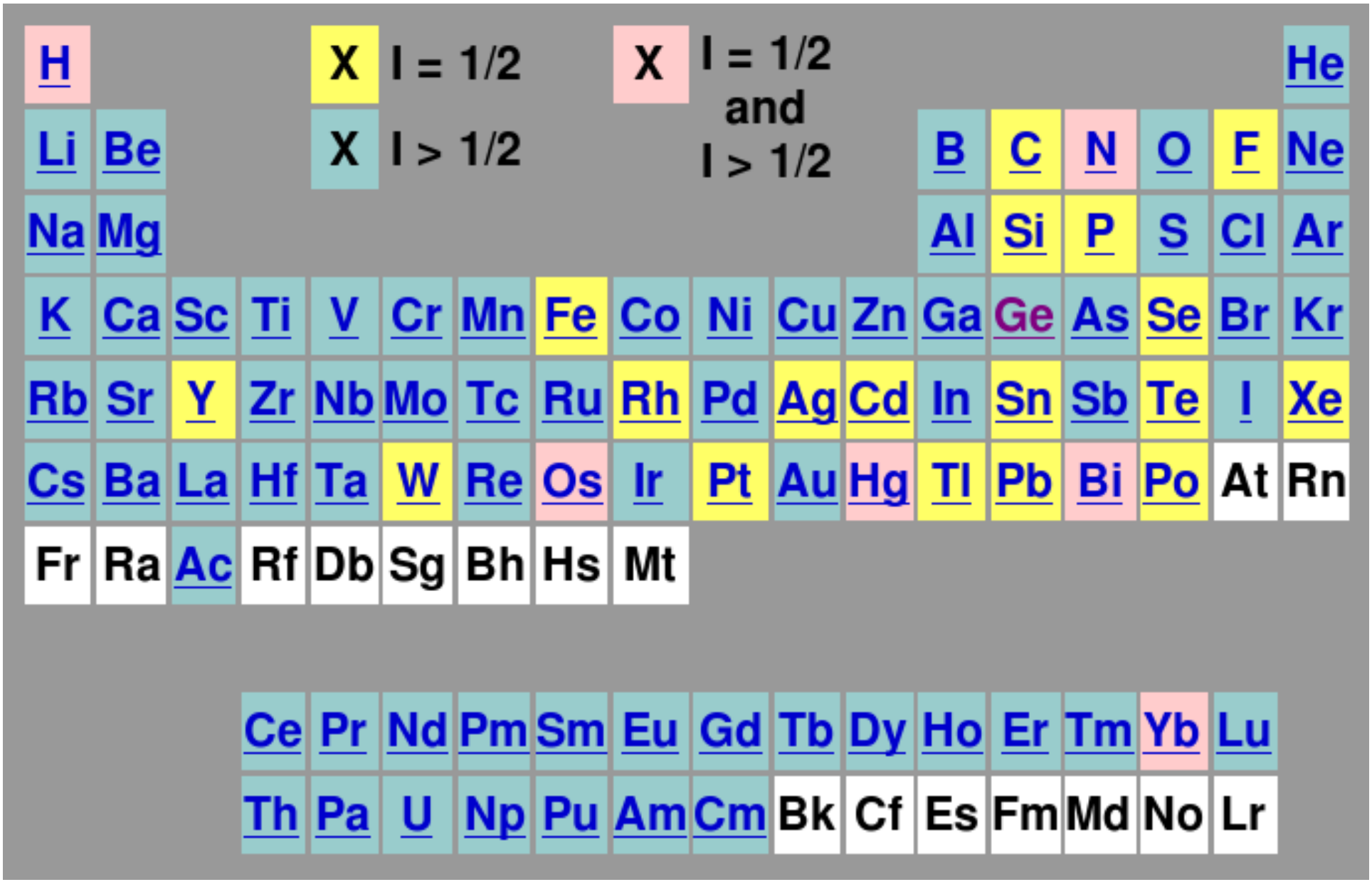

Nuclear spin and periodic table (2)

http://www.pascal-man.com/periodic-table/periodictable.html

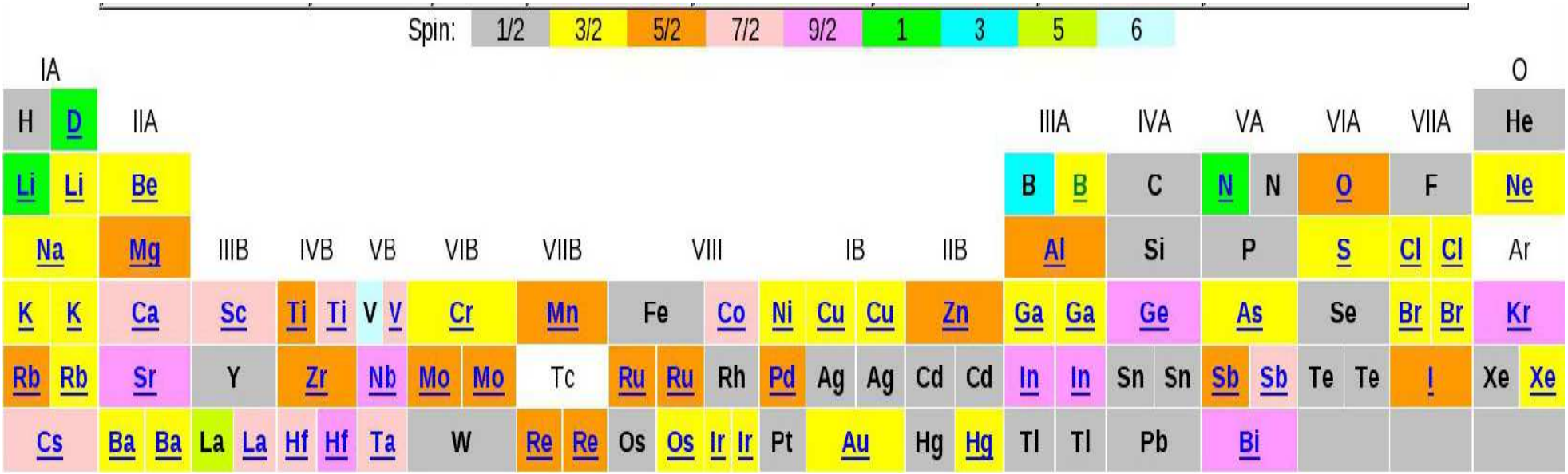

Most quadrupolar nuclei have half-integer spin

Electric Interactions: Quadrupole (1)

Nuclei with $I > 1/2$ have a non-spherical charge distribution and can interact with external electric fields. Classically, we have

$$E = qV = \int \rho(\mathbf{r}) V(\mathbf{r}) d\mathbf{r}$$

We can expand the potential term in series as

$$\begin{aligned} V(\mathbf{r}) &= V(0) + \sum_j \left.\frac{\partial V}{\partial x_j}\right|_{\mathbf{r}=\mathbf{0}} x_j + \frac{1}{2} \sum_{j,k} \left.\frac{\partial^2 V}{\partial x_j \, \partial x_k}\right|_{\mathbf{r}=\mathbf{0}} x_j \, x_k + \ldots \\ &= V(0) + \sum_j V_j x_j + \frac{1}{2} \sum_{j,k} V_{jk} x_j \, x_k + \ldots \end{aligned}$$

$V(0)$, V_j, V_{jk} are the potential, the electric field and electric field gradient, all calculated in $\mathbf{r} = \mathbf{0}$, hence they are numbers.
x_j, x_k are Cartesian coordinates

Electric Interactions: Quadrupole (2)

$$
\begin{aligned}
E &= \int \rho(\mathbf{r}) \left(V(0) + \sum_j V_j x_j + \frac{1}{2} \sum_{j,k} V_{jk} x_j \, x_k + \dots \right) d\mathbf{r} \\
&= qV(0) + \sum_j V_j \int \rho(\mathbf{r}) \, x_j d\mathbf{r} + \frac{1}{2} \sum_{j,k} V_{jk} \int \rho(\mathbf{r}) x_j \, x_k d\mathbf{r} + \dots
\end{aligned}
$$

- $qV(0)$ is a constant. Not important (we measure ΔE, not E)
- $\rho \, x_j d\mathbf{r}$ is an electric dipole. Never observed experimentally. Nuclear charge is distributed symmetrically
- $\rho \, x_j \, x_k \, d\mathbf{r}$ is a quadrupole moment. It appears if there is a non-zero electric field gradient, V_{jk}. It vanishes in highly symmetric environments

$\mathcal{H}_Q$: Definitions (1)

$$\mathcal{H}_Q = \frac{eQ}{2I(2I-1)\hbar}\,\mathbf{I}\cdot V\cdot\mathbf{I}$$

where

- I: spin quantum number
- eQ: electric Quadrupole moment
- V: EFG tensor
- $V_{zz}^P = eq$: magnitude of EFG gradient
- $V_{xx}+V_{yy}+V_{zz}=0$, hence in isotropic phases, $\mathcal{H}_Q$ does not contribute to the spectral frequencies.

In the PAS:

$$\mathcal{H}_Q = \frac{e^2qQ}{4I(2I-1)\hbar}\left[3\hat{I}^2_{z^{PAS}} - \hat{I}^2 + \eta(\hat{I}^2_{x^{PAS}} - \hat{I}^2_{y^{PAS}})\right]$$

Some references and a range of notations in literature [1, 2, 3, 4]

$\mathcal{H}_Q$: Definitions (2)

$$\chi = C_q = \frac{e^2 qQ}{\hbar} \qquad \eta = \frac{V^P_{xx} - V^P_{yy}}{V^P_{zz}}$$

$$\omega^P_Q = \frac{3\chi}{2I(2I-1)} \qquad P_Q = \chi\left(1 + \frac{\eta^2_Q}{3}\right)^{1/2}$$

$$\mathcal{H}_Q = \frac{\chi}{4I(2I-1)}\left[3\hat{I}^2_{z^{PAS}} - \hat{I}^2 + \eta(\hat{I}^2_{x^{PAS}} - \hat{I}^2_{y^{PAS}})\right]$$

$$= \frac{\chi}{2I(2I-1)} \sum_{k=-2}^{2} (-1)^k T_{2k} A_{2-k}$$

$$= \frac{\omega^P_Q}{3} \sum_{k=-2}^{2} (-1)^k T_{2k} A_{2-k}$$

$\mathcal{H}_Q$: Definitions (3)

$$\begin{aligned}\mathcal{H}_Q &= \frac{\omega_Q^P}{3}\sum_{k=-2}^{2}(-1)^k T_{2-k}A_{2k} \\ &= \frac{\omega_Q^P}{3}\sum_{k=-2}^{2}(-1)^k T_{2-k}\sum_j A_{2j}^P\, D_{jk}^{(2)}(\Omega^{PL})\end{aligned}$$

with

$$\mathbf{A^P} = \left\{\frac{\eta}{2}, 0, \sqrt{\frac{3}{2}}, 0, \frac{\eta}{2}\right\}$$

since it is often convenient to have the spin tensors in the lab frame when an external field is applied.

$\mathcal{H}_Q$: Interaction Frame Hamiltonian in high field

$$\mathcal{H} = \mathcal{H}_Z + \mathcal{H}_Q = \mathcal{H}_A + \mathcal{H}_B$$

If $\mathcal{H}_Q < \mathcal{H}_0$, in the high field approximation we can transform to the interaction frame

$$\begin{aligned}\tilde{\mathcal{H}}_Q(t) &= e^{i\omega_0 I_z t}\mathcal{H}_Q e^{-i\omega_0 I_z t} \\ &= \frac{\omega_Q^P}{3}\sum_{k=-2}^{2}(-1)^k A_{2k} T_{2-k} e^{i\omega_0 k t}\end{aligned}$$

It is useful to check convergence of $\bar{\mathcal{H}}_Q$ over one period.

$\bar{\mathcal{H}}_Q$ in high field (1)

$$\bar{\mathcal{H}}_Q = \bar{\mathcal{H}}_Q^{(1)} + \bar{\mathcal{H}}_Q^{(2)} + \ldots$$

For nuclei with $\mathcal{H}_Q \ll \mathcal{H}_Z$ it may be sufficient to use just $\bar{\mathcal{H}}_Q^{(1)}$

$$\begin{aligned}
\bar{\mathcal{H}}_Q^{(1)} &= \frac{\omega_Q^P}{3} A_{20}^L T_{20} \\
&= \frac{\omega_Q^P}{3} A_{20}^P \frac{1}{2} \left(3\cos^2\beta - 1 + \eta \sin^2\beta \cos 2\alpha\right) T_{20} \\
&= \frac{\omega_Q}{3} A_{20}^P T_{20}
\end{aligned}$$

with

$$\omega_Q = \omega_Q^P \frac{1}{2} \left(3\cos^2\beta - 1 + \eta \sin^2\beta \cos 2\alpha\right)$$

$\bar{\mathcal{H}}_Q$ in high field (2)

The energy levels are perturbed by

$$\begin{aligned}\bar{\mathcal{H}}_Q^{(1)} &= \frac{\omega_Q}{3} A_{20}^P T_{20} \\ &= \frac{\omega_Q}{3} A_{20}^P \left(3I_z^2 - I(I+1)\right)\end{aligned}$$

and the energy corrections are

$$\begin{aligned}\langle I,m|\,\bar{\mathcal{H}}_Q^{(1)}\,|I,m\rangle &= \frac{\omega_Q}{3} A_{20}^P \langle I,m|\,3I_z^2 - I(I+1)\,|I,m\rangle \\ &= \frac{\omega_Q}{3} A_{20}^P \left(3m^2 - I(I+1)\right)\end{aligned}$$

The energy changes to first order are the same for levels with the same $|m|$ values.

Energy diagram for integer quad spins

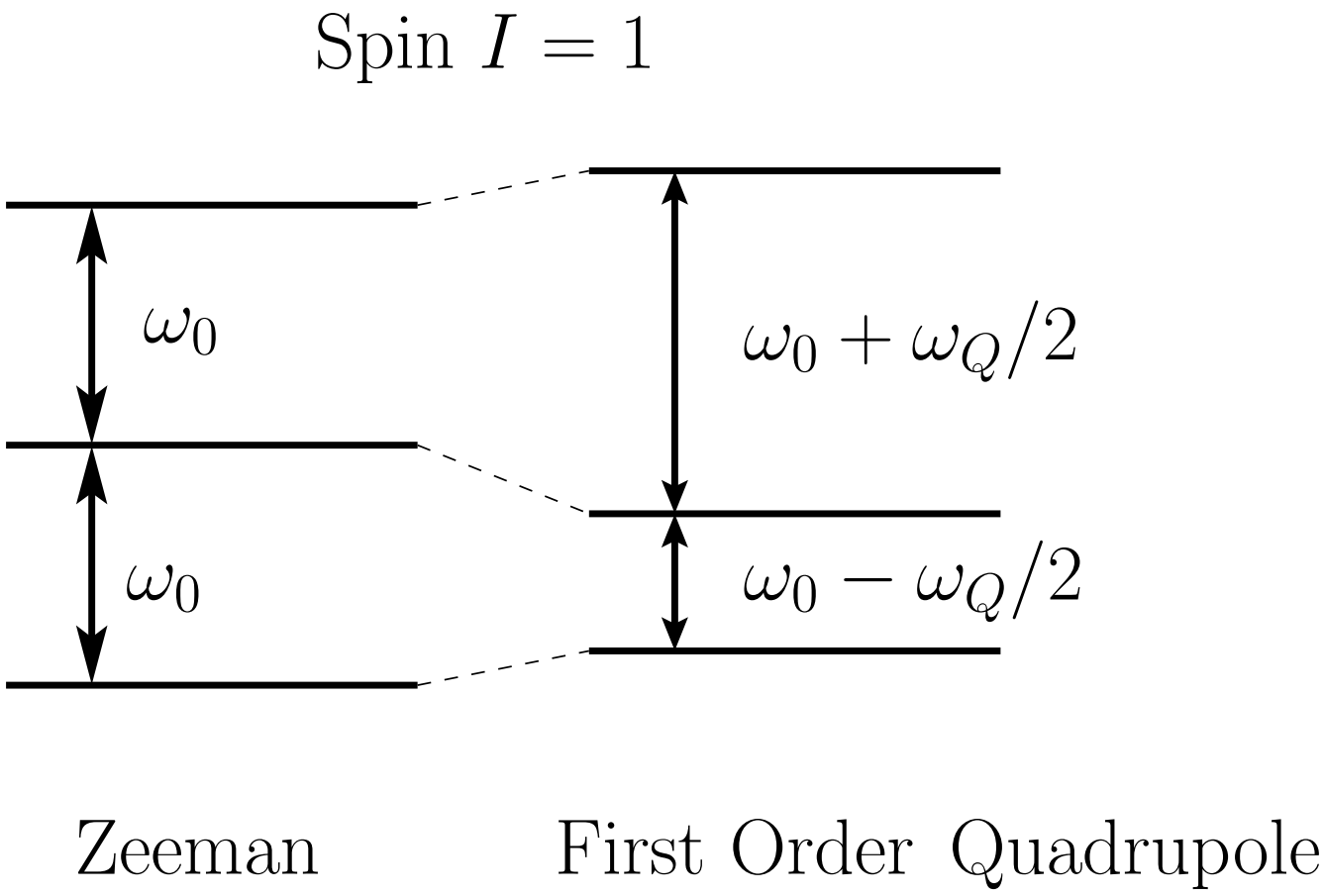

All transitions move are shifted from ω_0, which leads to significant complications if $\mathcal{H}_Q$ is large.

Spin $I = 1$ nuclei

^{2}H: Solid echo often used due to dead-time problems. Direct observation (2μs dead time) versus spin echo shown below

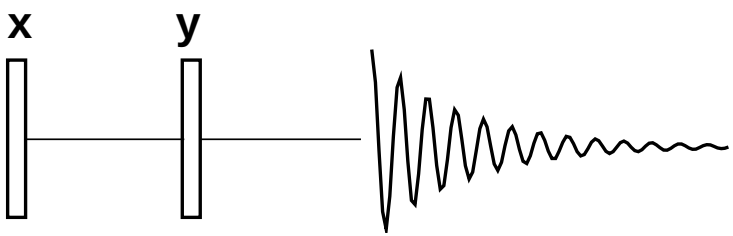

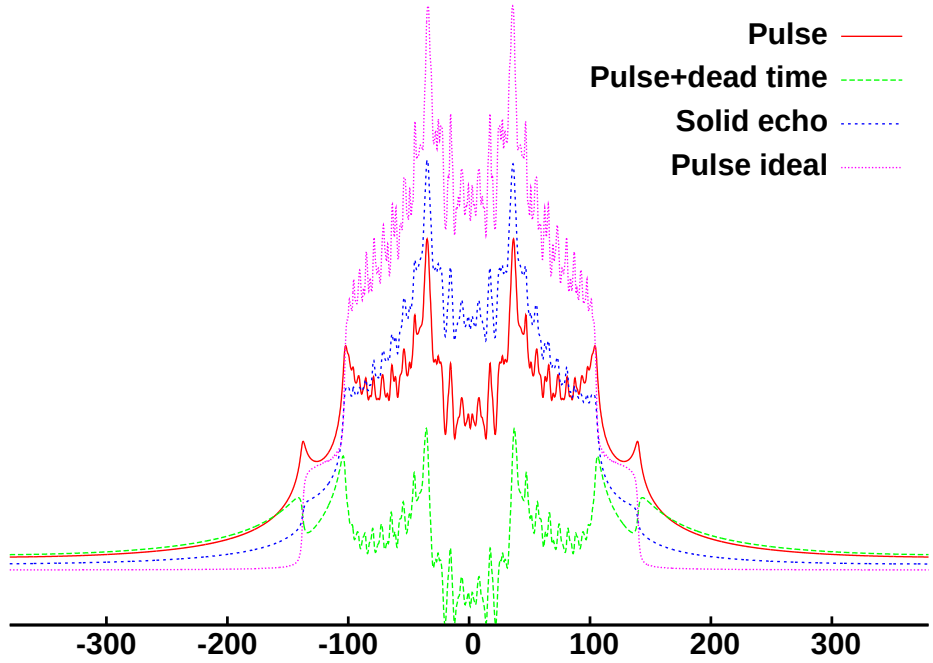

^{14}N: Large χ & low γ: tough to observe.

Recent revive through indirect observation & overtone NMR. NQR (nuclear Q resonance) to detect explosives.

Energy diagram for half-integer quad spins

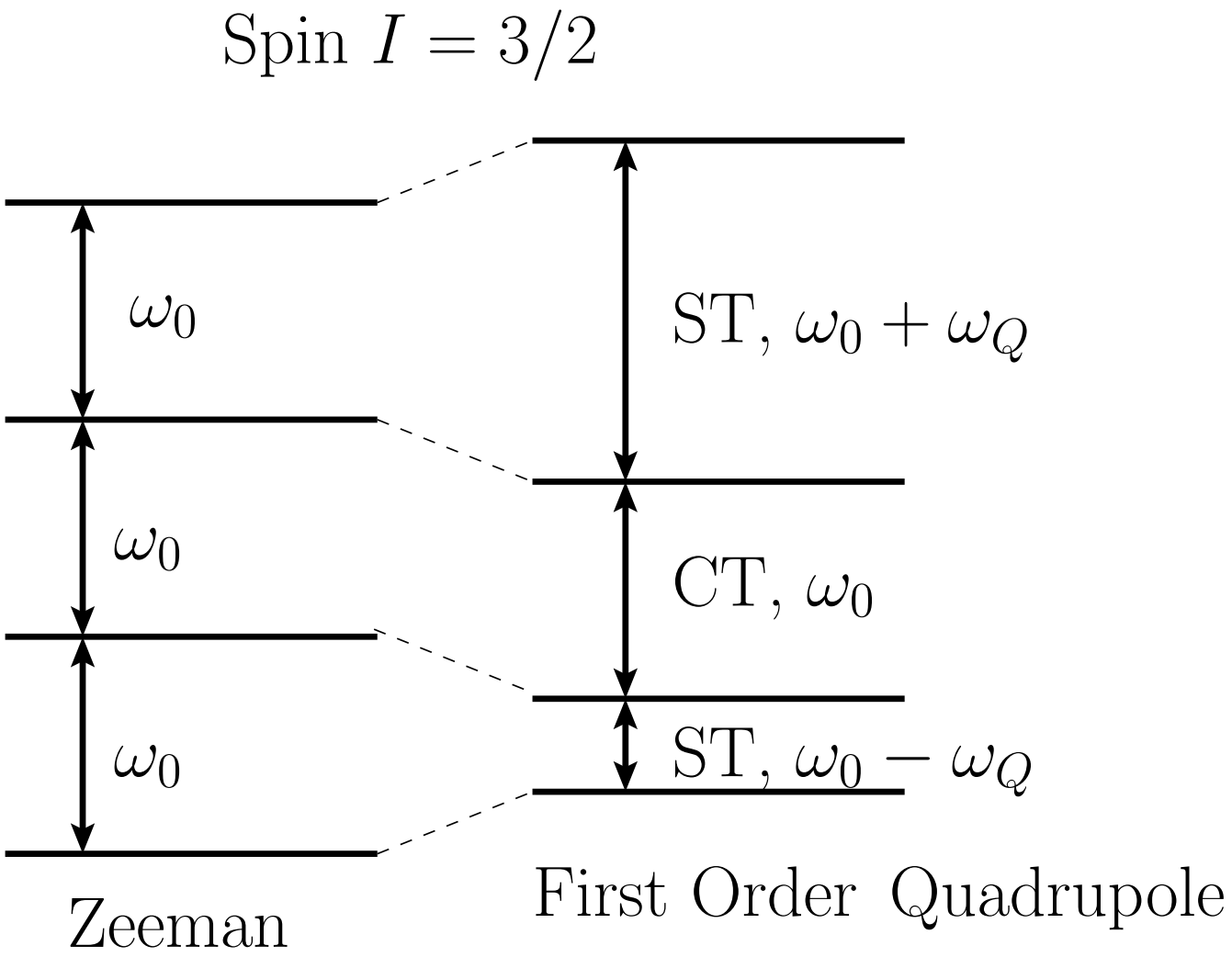

For half-integer spins, the CT between the $\pm 1/2$ levels is unaffected.

$\bar{\mathcal{H}}_Q$: Higher order terms (1)

$$\bar{\mathcal{H}}_Q = \bar{\mathcal{H}}_Q^{(1)} + \bar{\mathcal{H}}_Q^{(2)} + \dots$$

Convergence is often slow and may require often 2, sometimes 3, orders:

$$\begin{aligned}
\bar{\mathcal{H}}_Q^{(2)} &= \frac{1}{2i\tau_L}\int_0^{\tau_r} dt_2 \int_0^{t_2} [\mathcal{H}(t_2), \mathcal{H}(t_1)]\, dt_1 \\
&= \frac{1}{2i\tau_L}\left(\frac{\omega_Q^P}{3}\right)^2 \sum_{j,k} (-1)^{k+j} A_{2k} A_{2j} \left[T_{2-k}, T_{2-j}\right] \times \\
&\quad \times \int_0^{\tau_L} dt_2 \int_0^{t_2} e^{i\omega_0(kt_2+jt_1)} dt_1
\end{aligned}$$

$\bar{\mathcal{H}}_Q$: Higher order terms (2)

$$
\begin{aligned}
\bar{\mathcal{H}}_Q^{(2)} &= \frac{(\omega_Q^P)^2}{9\omega_0} \sum_{k\neq 0} \frac{1}{k} \left(A_{2k} A_{2-k} \left[T_{2k}, T_{2-k} \right] + A_{2k} A_{20} \left[T_{2k}, T_{20} \right] \right) \\
&\approx \frac{(\omega_Q^P)^2}{9\omega_0} \sum_{k\neq 0} \frac{1}{k} A_{2k} A_{2-k} \left[T_{2k}, T_{2-k} \right] \\
&= \frac{(\omega_Q^P)^2}{9\omega_0} \sum_{k\neq 0} \frac{1}{k} \sum_{J=0}^{4} \sum_{j=0}^{4} C(2,2,J;k,-k) \mathcal{A}_{J0} \times \\
&\quad \left\{ C(2,2,j;k,-k) - C(2,2,j;-k,k) \right\} T_{j0} \\
&= \frac{(\omega_Q^P)^2}{9\omega_0} \sum_{J=0}^{4} \sum_{j=1,3} \rho_{Jj} \, \mathcal{A}_{J0} \, T_{j0}
\end{aligned}
$$

$\bar{\mathcal{H}}_Q$: Higher order terms (3)

Since the quadrupolar tensor is real and symmetric, only the spatial terms with even rank are non-zero

$$\bar{\mathcal{H}}_Q^{(2)} = \frac{(\omega_Q^P)^2}{9\omega_0} \sum_{J=0,2,4} \sum_{j=1,3} \rho_{Jj}\, \mathcal{A}_{J0}\, T_{j0}$$

where

- second-order isotropic shift of $\bar{\mathcal{H}}_Q^{(2)}$ coming from $\mathcal{A}_{00}$ is [3]

$$\omega_{iso}^{(2)} \propto \frac{1}{30} \frac{(\omega_Q^P)^2}{\omega_0} \left(I(I+1) - \frac{3}{4} \right) \left(1 + \frac{\eta^2}{3} \right)$$

- $\mathcal{A}_{20}$ and $\mathcal{A}_{40}$ are rank 2 and 4 tensors (see [4] for expression in their PAS)

Energy diagram for half-integer spins

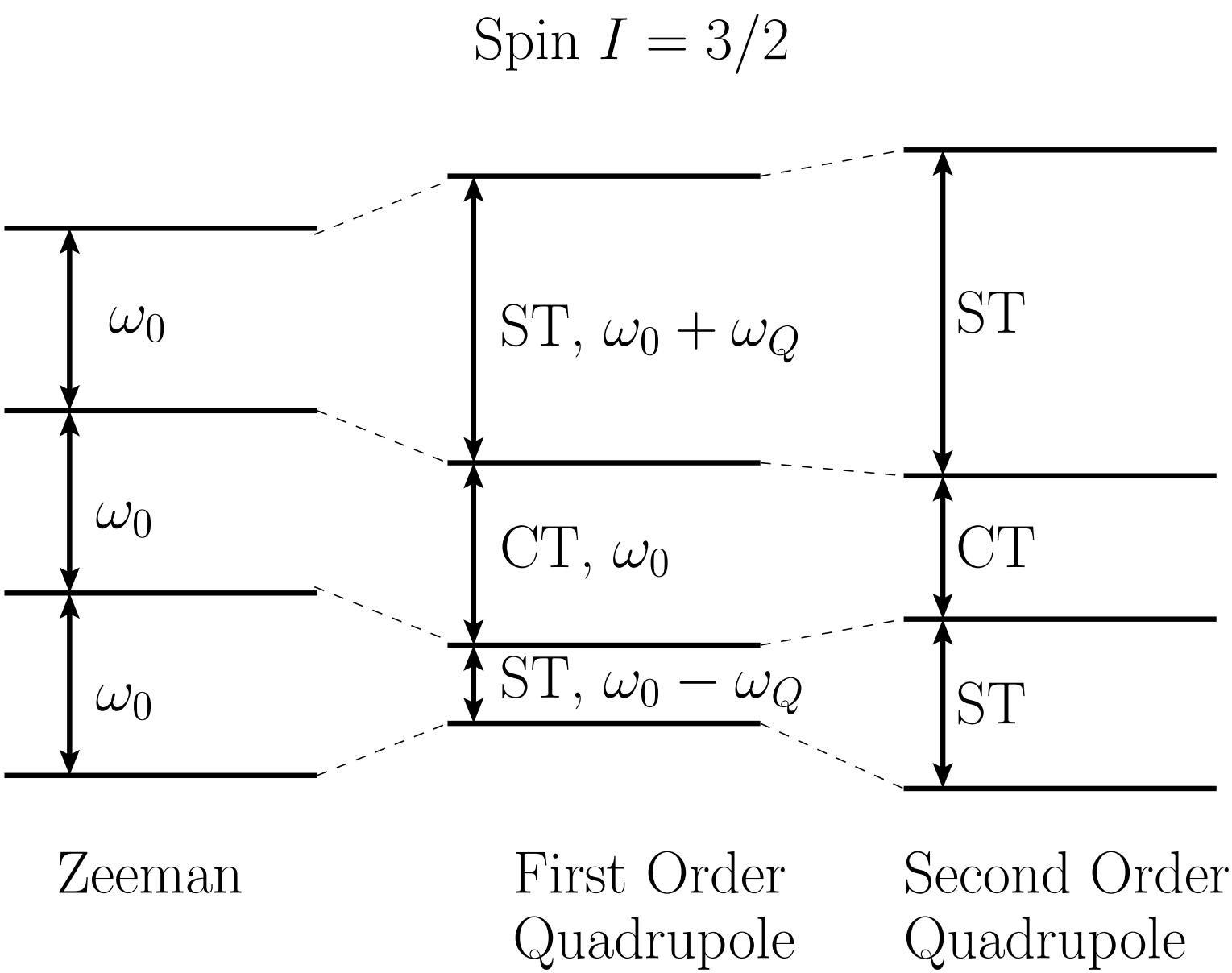

Simulated full spectrum for $^{87}RbClO_4$

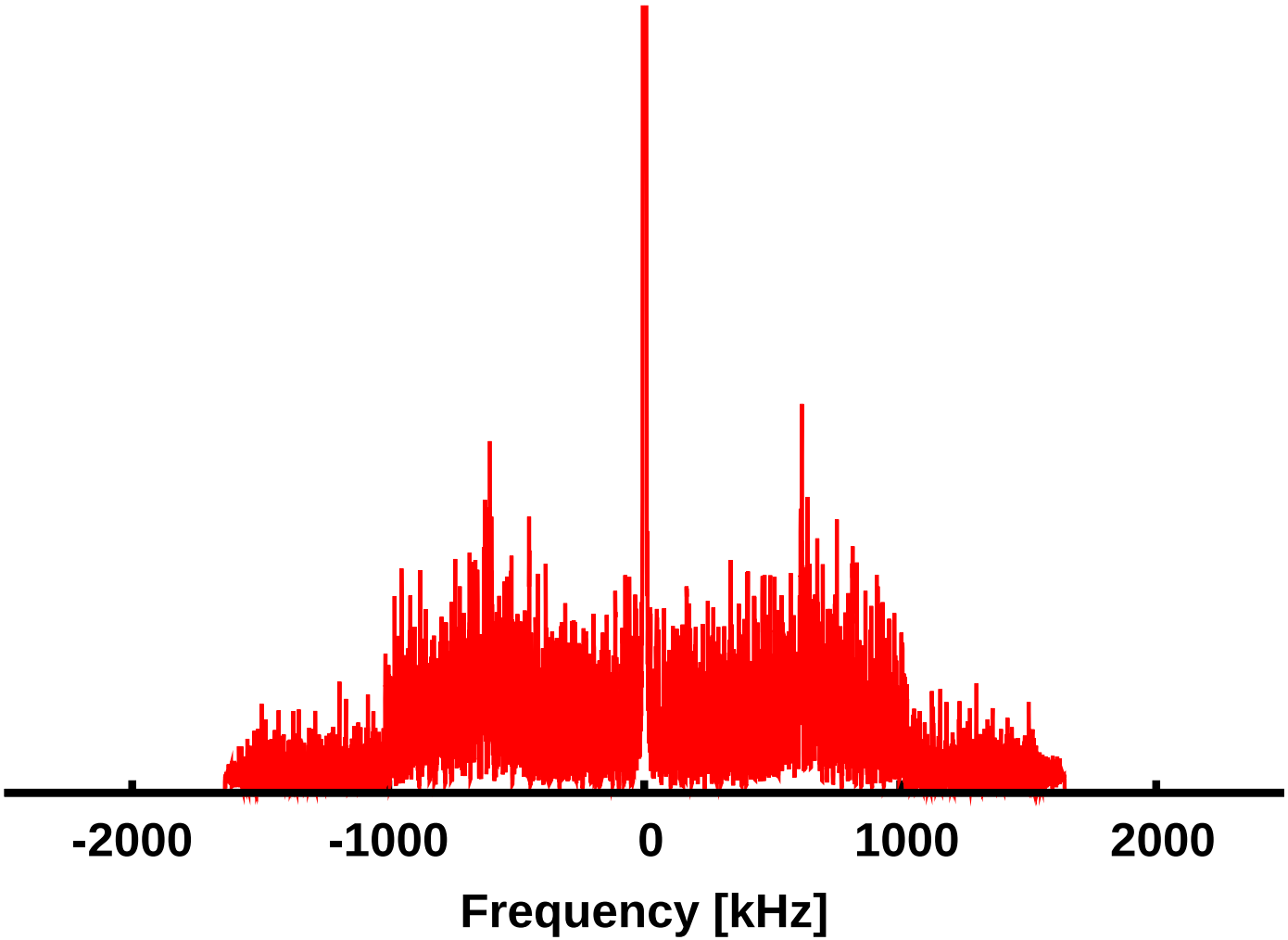

Quadrupolar parameters in simpson file on BB, Ref. [5].

CT with first and second order $\bar{\mathcal{H}}_Q^{(n)}$

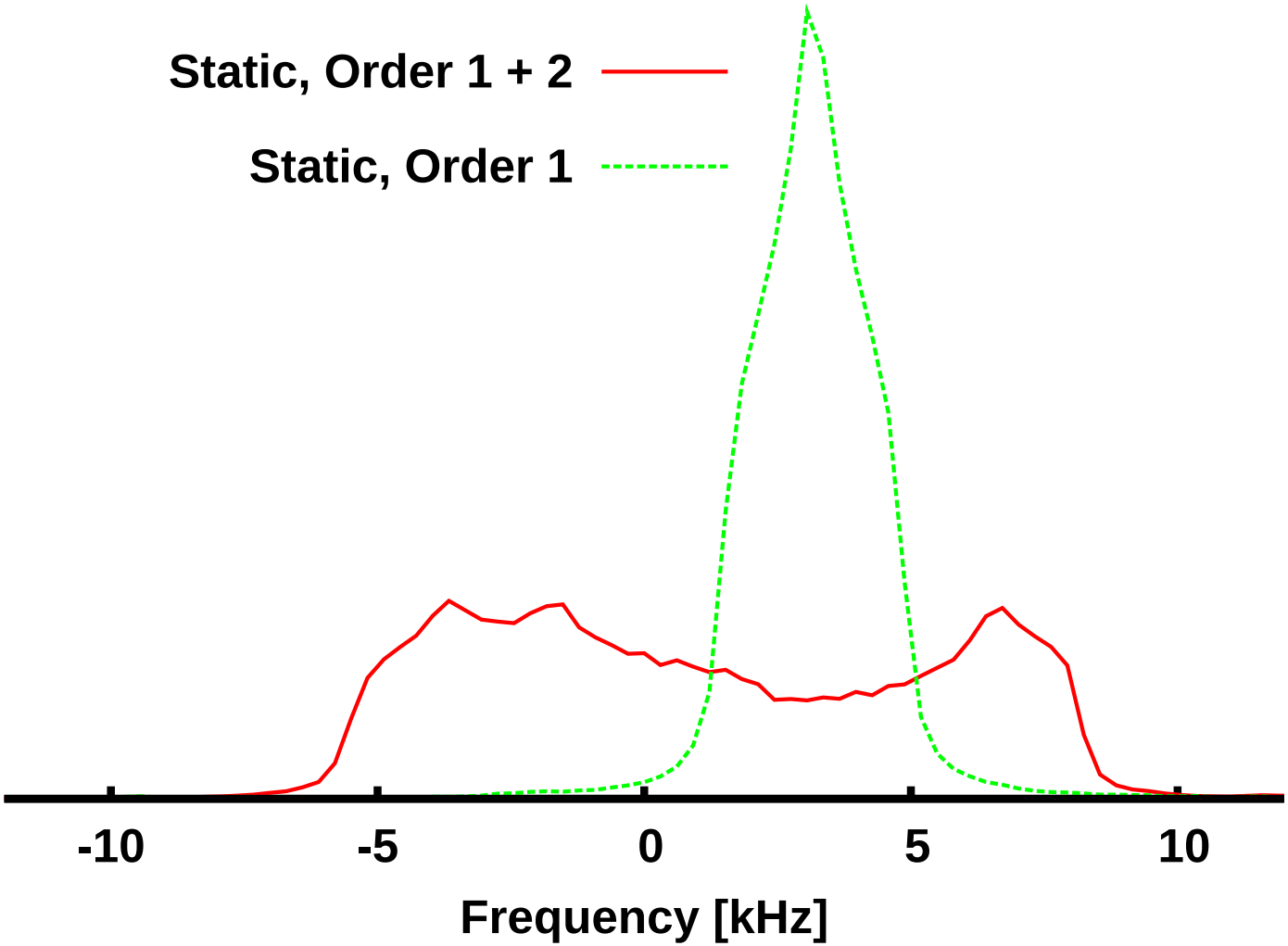

Nutation curves & Quadrupole

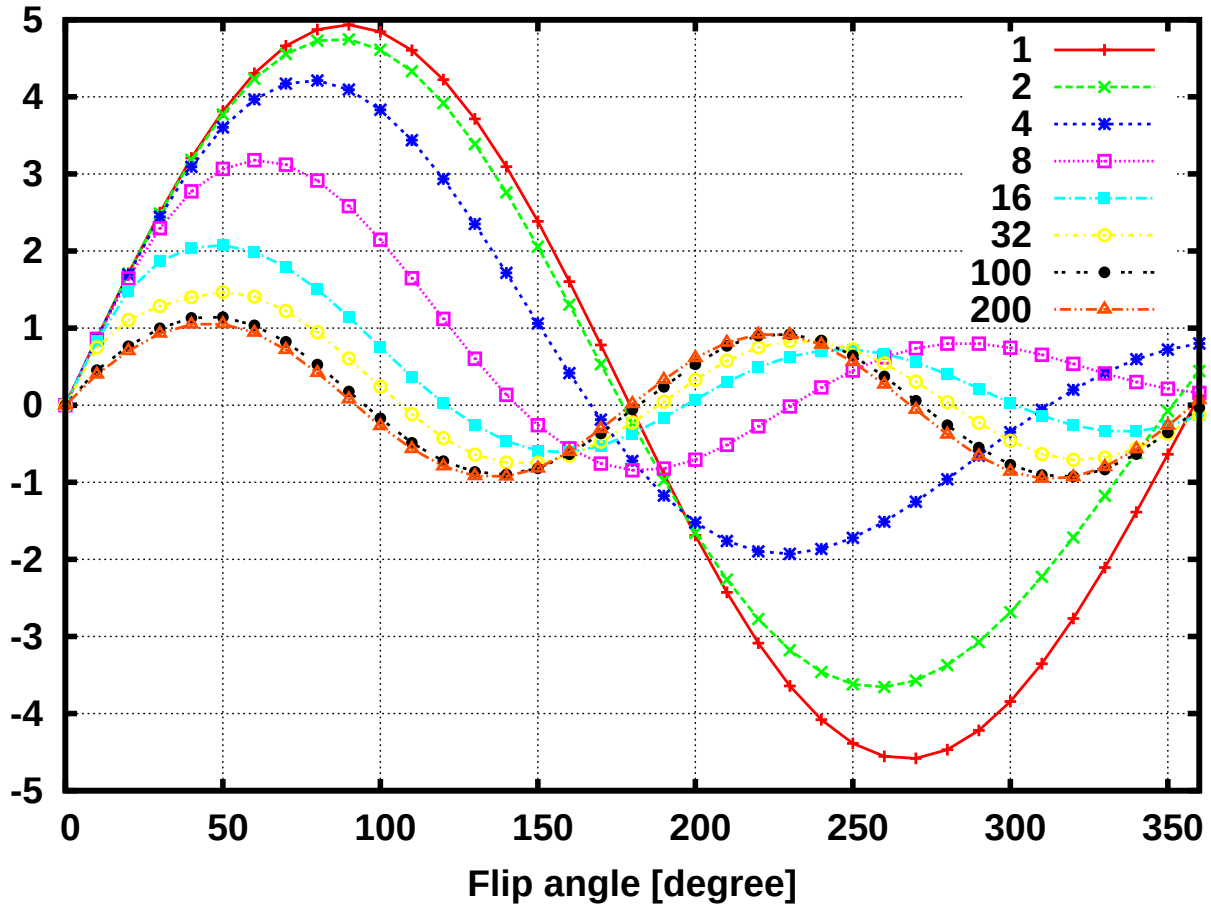

$$Label = \frac{\omega_Q^P}{\omega_{nut}^{hard}}$$

$$\omega_{nut}^{hard} = \gamma B_1$$

$$\omega_{nut}^{soft} = \gamma B_1 (I + \frac{1}{2})$$

For excitation over a wide ω_Q range and meaningful intensities, small flip angles are best (i.e., 30^o)

$\bar{\mathcal{H}}_Q$: high field & sample rotation (1)

$$\begin{aligned}
\mathcal{H}_Q(t) &= \bar{\mathcal{H}}_Q^{(1)} + \bar{\mathcal{H}}_Q^{(2)} \\
&= \frac{\omega_Q^P}{3} \sum_{m=-2}^{2} A_{2m}^R \, D_{m0}^{(2)}(\omega_r t + \alpha_0, \beta_R, \gamma_0) \, T_{20} + \\
&\quad \frac{\omega_Q^2}{9\omega_0} \sum_{J=0,2,4} \sum_{j=1,3} \sum_{M=-J}^{J} \rho_{Jj} \, \mathcal{A}_{JM}^R \, D_{M0}^{(J)}(\omega_r t + \alpha_0, \beta_R, \gamma_0) \, T_{j0}
\end{aligned}$$

Under fast rotation, all time-dependent terms vanish over τ_r to first order, hence only $m = 0$ and $M = 0$ survive

$$\begin{aligned}
\bar{\mathcal{H}}_Q &= \frac{\omega_Q^P}{3} A_{20}^R \, d_{00}^{(2)}(\beta_R) \, T_{20} + \\
&\quad \frac{\omega_Q^2}{9\omega_0} \sum_{J=0,2,4} \sum_{j=1,3} \rho_{Jj} \, \mathcal{A}_{J0}^R \, d_{00}^{(J)}(\beta_R) \, T_{j0}
\end{aligned}$$

$\bar{\mathcal{H}}_Q$: high field & sample rotation (2)

The reduced Wigner matrix d^2_{00} and d^4_{00} coincide with the Legendre polynomials ($z = \cos\beta$):

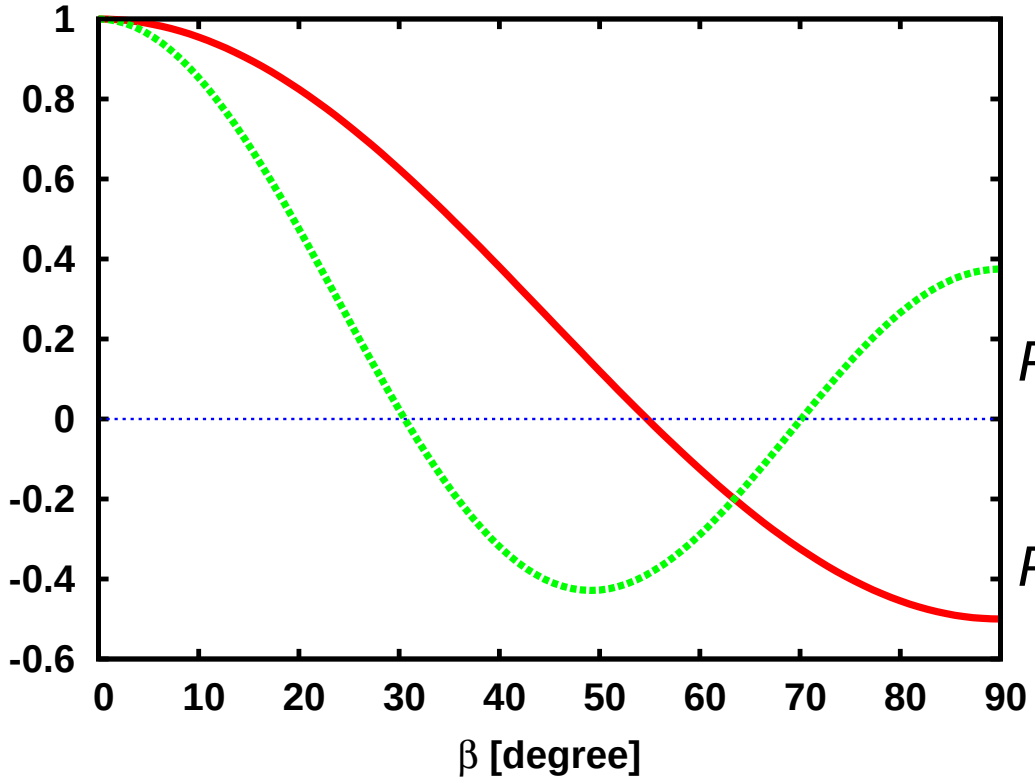

Legendre polynomials

$$P_2(z) = \frac{3z^2 - 1}{2}$$

$$P_4(z) = \frac{35z^4 - 30z^2 + 3}{8}$$

where $P_2(\cos 54.74^\circ) = 0$ and $P_4(\cos 30.56^\circ) = P_4(\cos 70.12^\circ) = 0$

$\bar{\mathcal{H}}_Q$: high field & sample rotation (3)

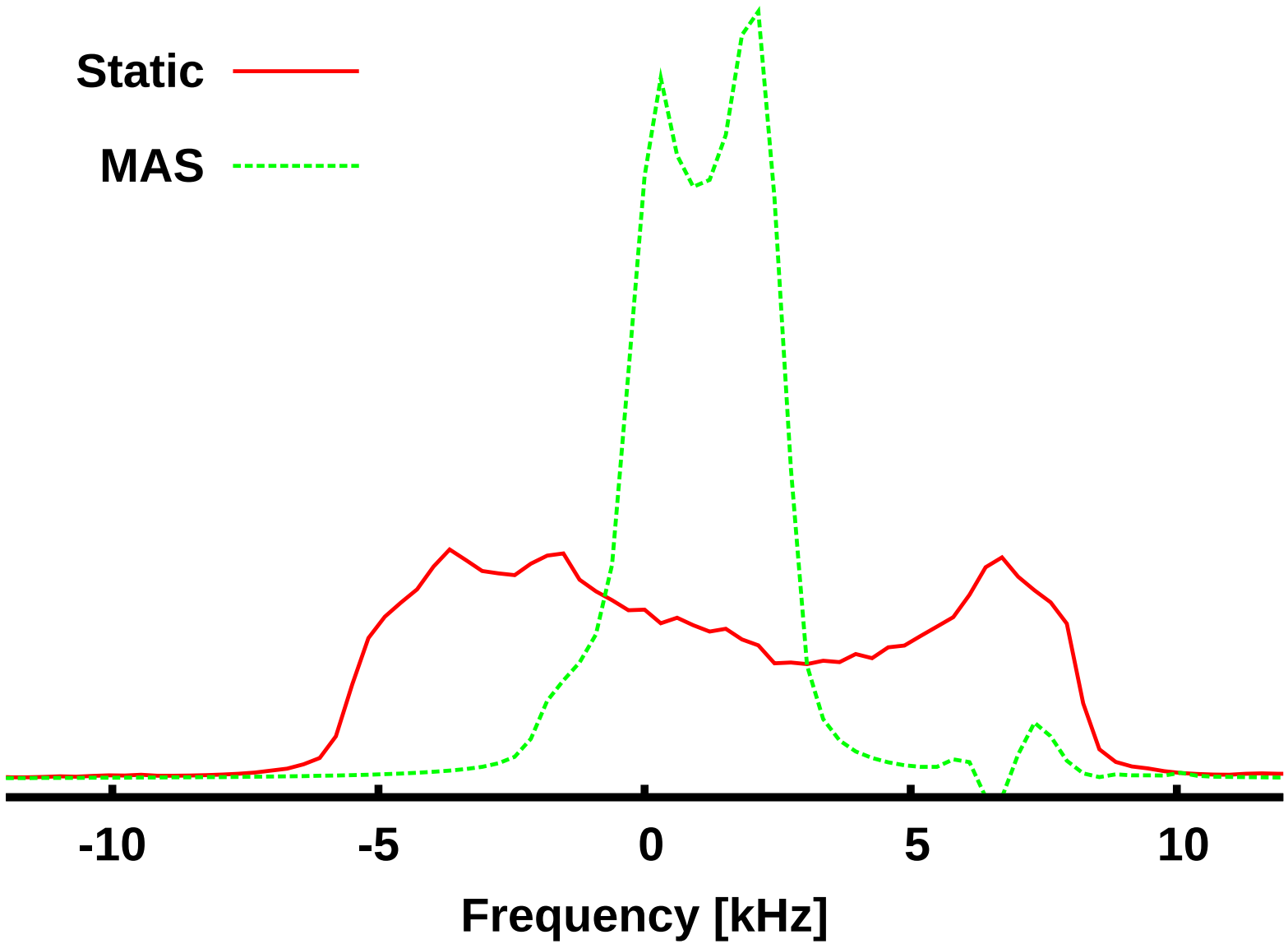

Removal of second order broadening under rotation

MAS alone can not produce high resolution spectra.

- At the magic angle, rank 2 spatial tensors are eliminated
- Rank 2 and rank 4 space terms vanish at different angles

Alternative approaches are needed

- Mechanical:
  - DOR (Double rotation) [6]
  - DAS (Dynamic angle spinning) [7]
- Pulse sequences:
  - MQMAS
  - STMAS

DOR (1)

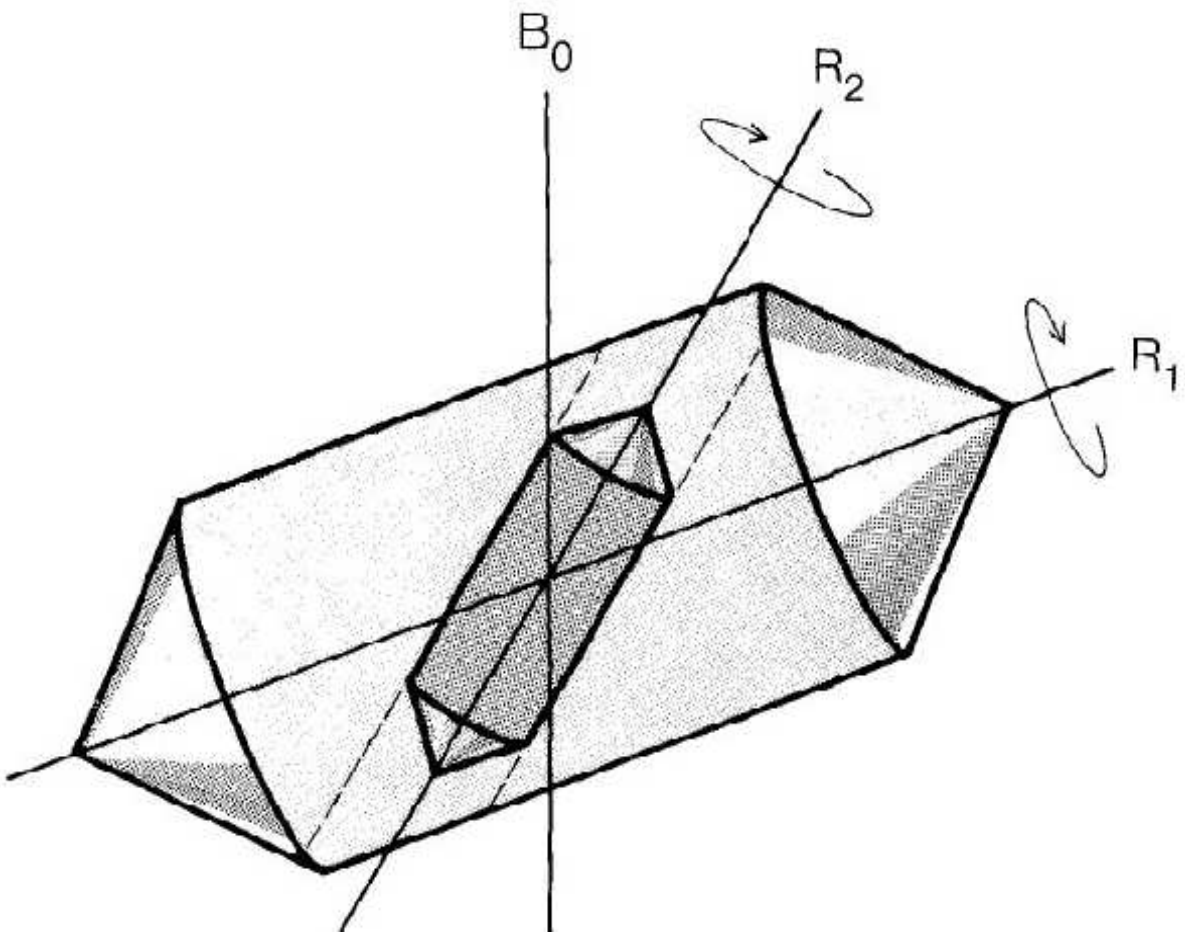

For instance

$\beta_2 = 54.74^o$

$\beta_1 = 30.56^o$

To achieve high resolution, the rotations are aimed at suppressing the $P_2(\cos\beta_2)$ and $P_4(\cos\beta_1)$ Legendre polynomials.

DOR (2)

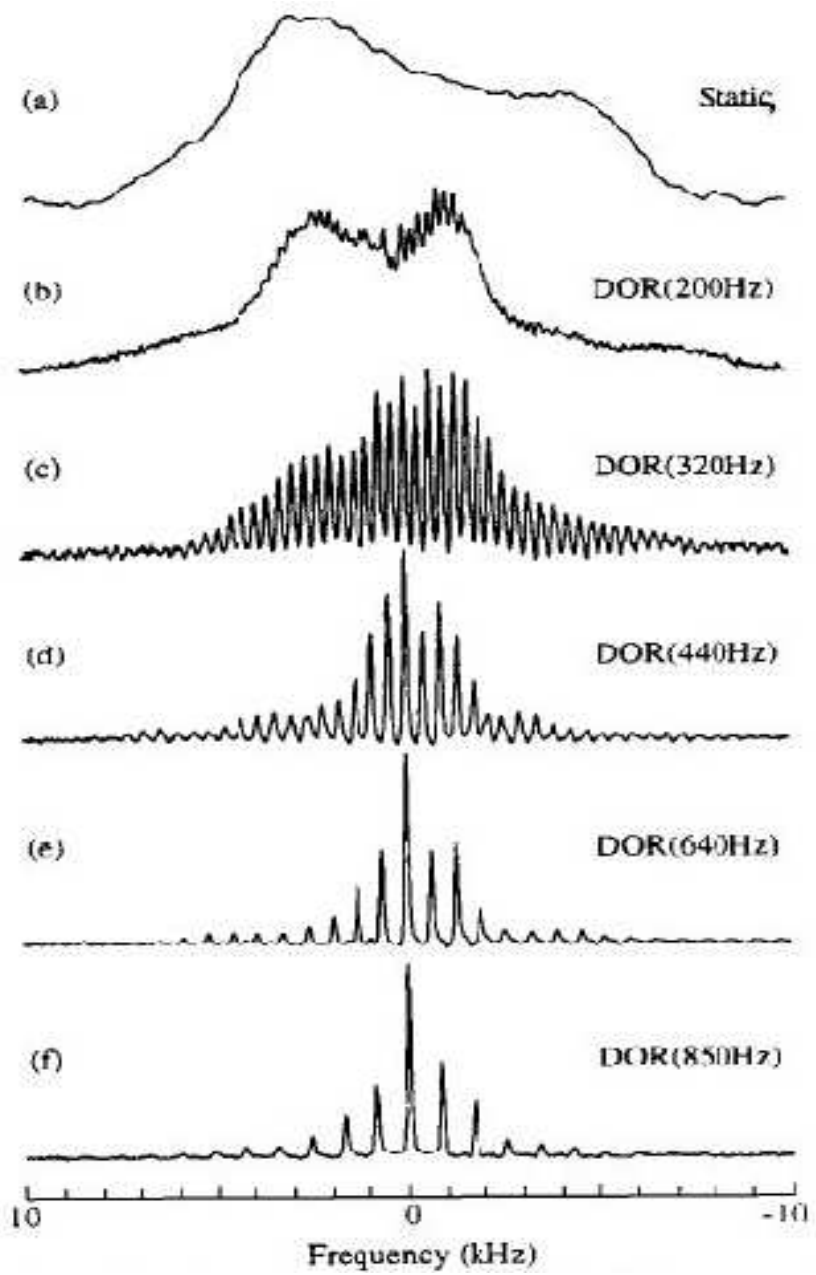

Rotation around R_2 is moderately fast.

Rotation around R_2 is a lot slower, and gives rise to the ssb visible in the DOR spectrum [4].

^{23}Na NMR on sodium oxalate, outer rotor=400-900Hz; inner rotor=4 kHz

These ssb can also be partly eliminated [8, 9]

DAS

The sample is spun at β_1, during t_1 and β_2 during t_2, by suddenly flipping the rotation axis of the sample [7, 1].

$\omega_{-\frac{1}{2}\leftrightarrow\frac{1}{2}}$ oscillates w.r.t the spinning axis β in $[0^o, 90^o]$ and depends on the orientation of the PAS.

If the oscillation curves are scaled by their value at certain angles, there exist certain pairs $\{\beta_1, \beta_2\}$ at which $\omega_{-\frac{1}{2}\leftrightarrow\frac{1}{2}}(\beta_1) \propto \omega_{-\frac{1}{2}\leftrightarrow\frac{1}{2}}(\beta_2)$

$$\begin{aligned} P_2(\cos\beta_1)t_1 + P_2(\cos\beta_2)t_2 &= 0 \\ P_4(\cos\beta_1)t_1 + P_4(\cos\beta_2)t_2 &= 0 \end{aligned}$$

There are no solutions in $\beta \in (39.23^o, 63.43^o)$, hence none at the magic angle.

MQMAS (1)

MQMAS was a major breakthrough in the field. High resolution information can be obtained without specialised equipment [10].

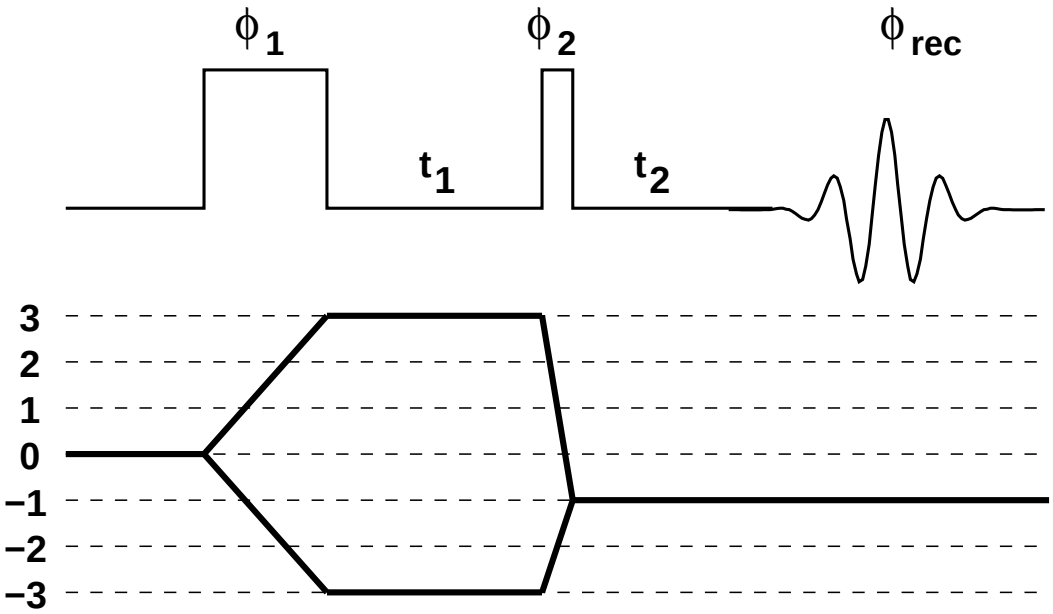

MQMAS refocuses undesired terms generated in t_1 under a time $t_2 = kt_1$ by correlating SQ and MQ transitions.

MQMAS (2)

The symmetric transitions are given by [3, 10]:

$$\omega_{-m\leftrightarrow m} = \frac{(\omega_Q^P)^2}{\omega_0} \sum_{J=0,2,4} A_J C_J(I,m) P_J(\cos\beta)$$

where $C_J(I,m)$ are simple expressions which depend on the spin quantum numbers.

MQMAS experiments use these $C_J(I,m)$ values to generate an "echo" such that rank-4 terms are cancelled by setting

$$t_2 = \left| \frac{C_4(I,m)}{C_4(I,\frac{1}{2})} \right| t_1$$

MQMAS (3)

MQMAS spetra need to be specially processed, a procedure called shearing. [11]

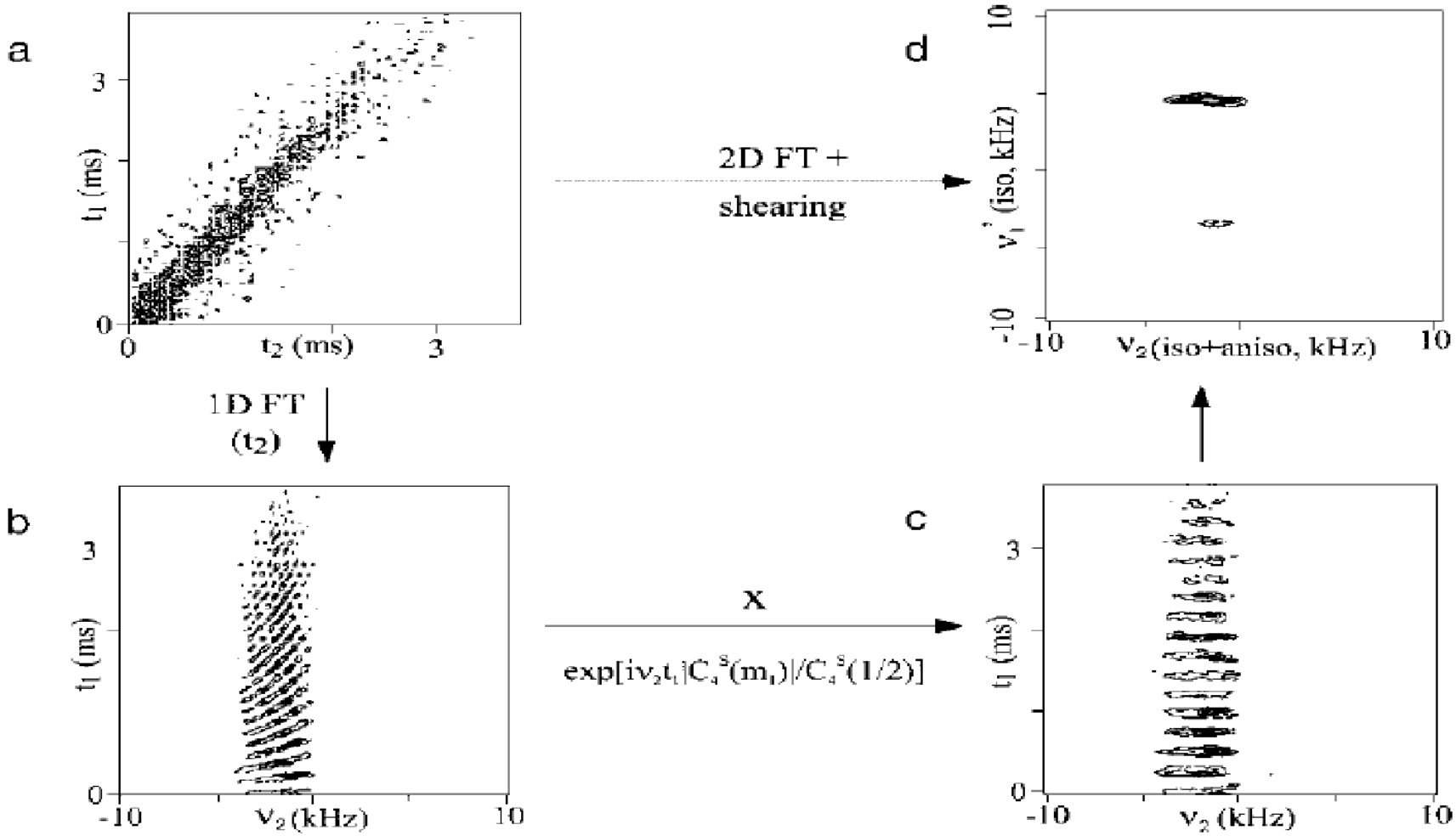

MQMAS (4)

Some general considerations:

- The efficiency of MQMAS is in general quite low.
- The MQ efficiency goes down with higher quantum orders.
- The efficiency improves very steeply when with the nutation frequency of the exciting rf pulses.
- The original MQMAS sequence gives 2D spectra which are not in pure absorption.
- Modifications of this sequence lead to spectra with a pure absorption phase.

Split-t_1 Whole Echo MQMAS sequence

For sites with relatively long T_2, the acquisition of a whole echo [12, 13] boosts the signal and provides pure phase absorption line shapes [3]. Some versions of this experiment require no shearing needed.

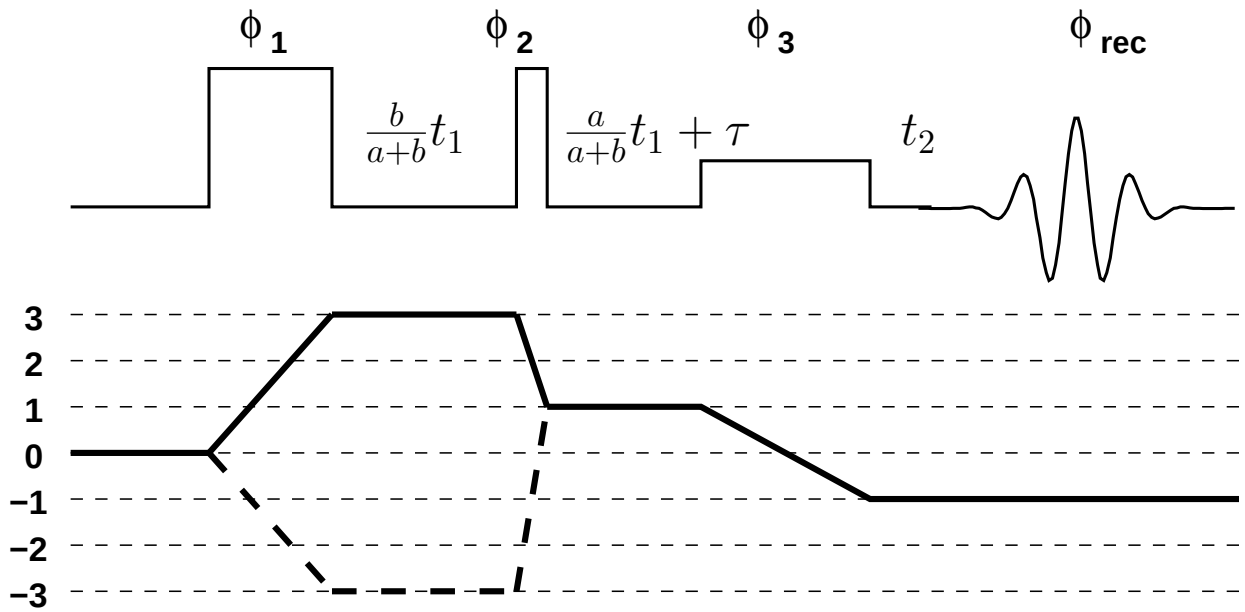

Z-filtered MQMAS sequence

This is a very robust sequence [14, 3] with can be used on samples with both long and very short T_2. It needs shearing.

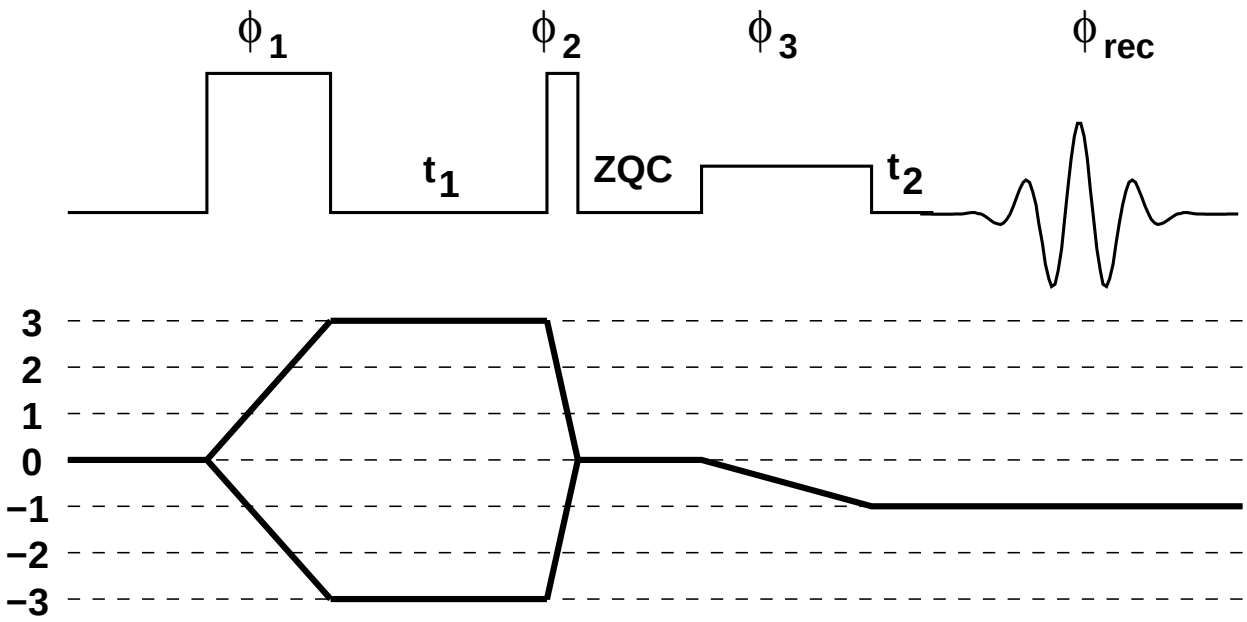

3QMAS of $^{87}RbNO_3$ at 4.7 T & 10 kHz

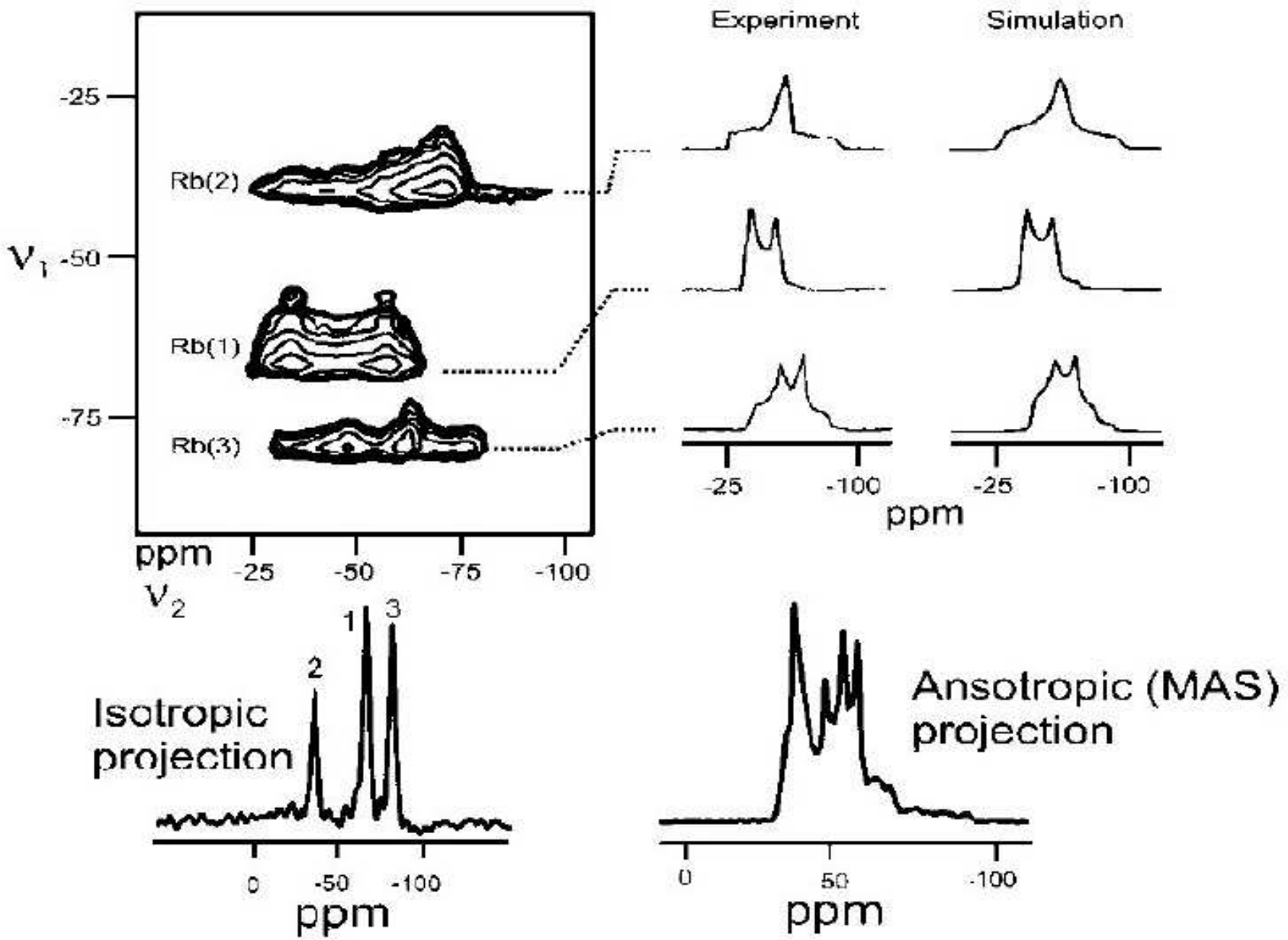

Enhancement schemes for MQMAS signal (1)

There are many schemes to enhance the MQMAS signal (some for spin 3/2 below).

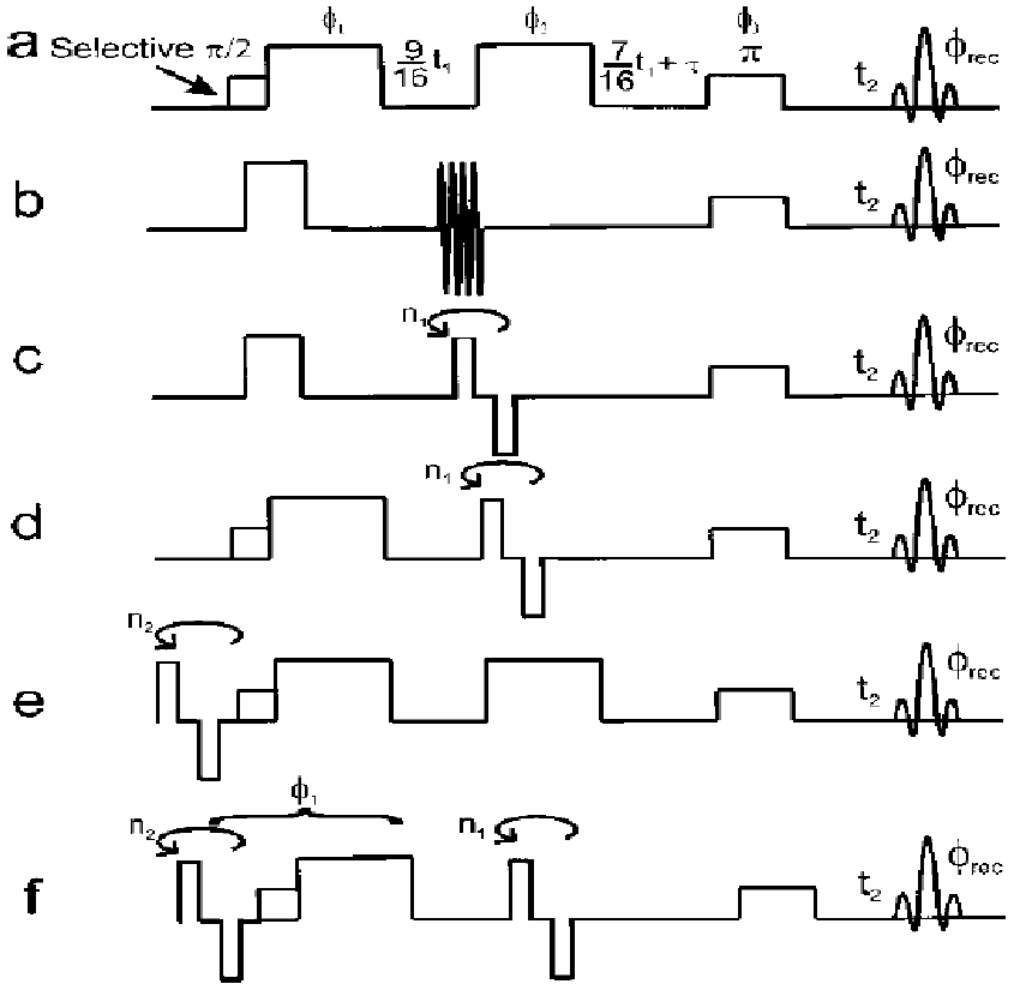

Enhancement schemes for MQMAS signal (2)

Enhancement schemes applied to $^{87}RbNO_3$ [3]

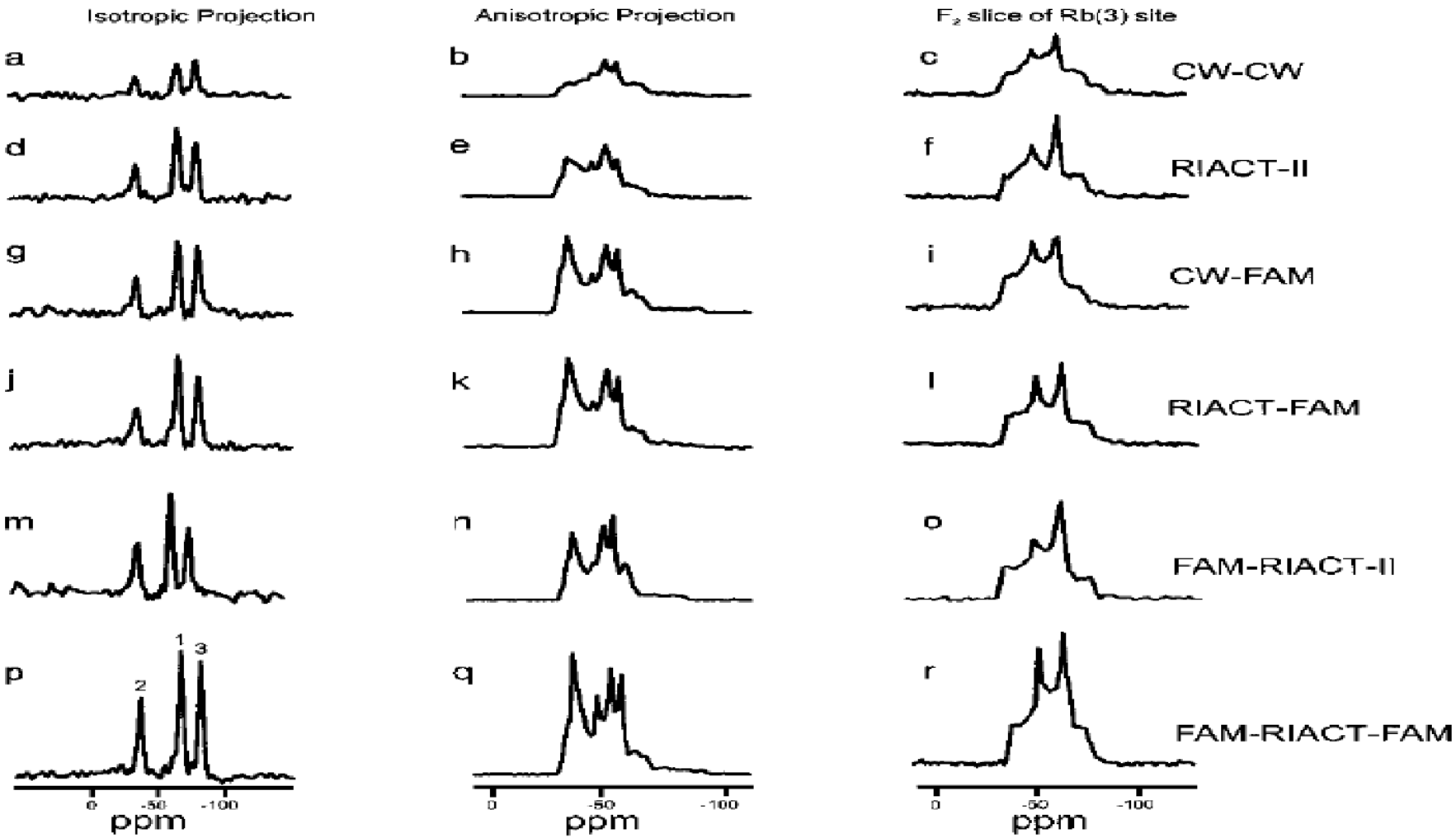

STMAS (1)

High resolution spectra are obtained by correlating ST and CT [15, 16].

These experiments are typically

- More tricky to set up, as may suffer from magic-angle missets [17]
- More efficient than the MQMAS (poor MQ excitation efficiency)
- Resolution in second dimension typically not as good as MQMAS

STMAS (2)

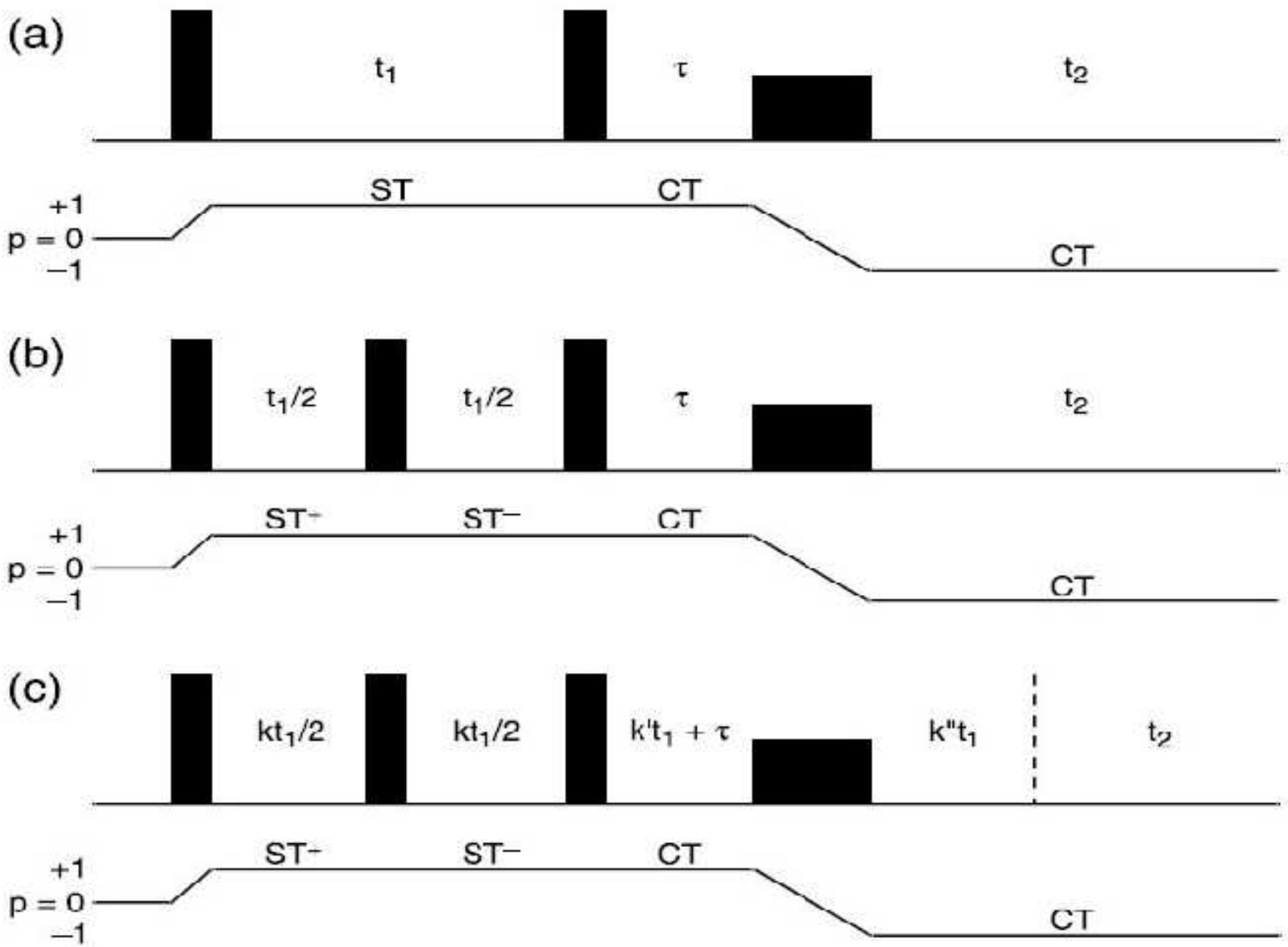
(a)
t_1
τ
t_2
ST
CT
CT
+1
p = 0
−1
(b)
$t_1/2$
$t_1/2$
τ
t_2
ST−
ST−
CT
CT
+1
p = 0
−1
(c)
$kt_1/2$
$kt_1/2$
$k't_1 + \tau$
$k''t_1$
t_2
ST−
ST−
CT
CT
+1
p = 0
−1

Quadrupole size and optimal approach

A wide range of approaches may be needed depending on the system under investigation [2].

- $\chi_Q < 0.7$ MHz, it is possible to acquire the spectrum with pulse-acquire method. MAS simulation of centerband can provide parameters.
- If the second order broadening is large, acquire with a Hahn echo with selective pulses to observe CT, short τ, preferably rotor synchronised

Selected Reading (1)

[1] M. J. Duer, *Solid State NMR Speectroscopy, Principles and Applications*, Blackwell Science (UK), (2002).

[2] K. J. D. MacKenzie and M. E. Smith, *Multinuclear solid-state NMR of inorganic materials*, Pergamon, (2002).

[3] A. Goldbourt and P. K. Madhu, *Monatsh. Chem.* **346**, 1–38 (2002).

[4] B. Q. Sun, J. H. Baltisberger, Y. Wu, A. Samoson and A. Pines, *Solid State Nucl. Magn. Reson.* **1**, 267 – 295 (1992).

[5] F. H. Larsen, H. J. Jakobsen, P. D. Ellis and N. C. Nielsen, *J. Phys. Chem. A* **101**, 8597–8606; (1997).

[6] A. Samoson, E. Lippmaa and A. Pines, *Mol. Phys.* **65**, 1013 (1988).

[7] K. T. Mueller, B. Q. Sun, G. C. Chingas, J. W. Zwanziger, T. Terao and A. Pines, *J. Magn. Reson.* **86**, 470–487 (1990).

[8] A. Samoson, *Chem. Phys. Lett.* **214**, 456 – 458 (1993).

Selected Reading (2)

[9] A. Samoson and J. Tegenfeldt, *J. Magn. Reson. A* **110**, 238–244 (1994).

[10] L. Frydman and J. S. Harwood, *J. Am. Chem. Soc.* **117**, 5367–5368 (1995).

[11] A. Medek, J. S. Harwood and L. Frydman, *J. Am. Chem. Soc.* **117**, 12779 (1995).

[12] D.Massiot, B.Touzo, D.Trumeau, J.P.Coutures, J.Virlet, P.Florian and P.J.Grandinetti, *Solid State Nucl. Magn. Reson.* **6**, 73–83 (1996).

[13] S. P. Brown and S. Wimperis, *J. Magn. Reson.* **124**, 279–285 (1997).

[14] J.-P. Amoureux, C. Fernandez and S. Steuernagel, *J. Magn. Reson.* **123**, 116–118 (1996).

[15] Z. Gan, *J. Am. Chem. Soc.* **122**, 3242 (2000).

[16] S. E. Ashbrook and Stephen Wimperis, *Progr. Nucl. Magn. Res. Spectr.* **45**, 53–108 (2004).

Selected Reading (3)

[17] S. E Ashbrook and S. Wimperis, *J. Magn. Reson.* **162**, 402 – 416 (2003).